# Thermodynamic and kinetic constants for isotopic fractionation modeling with or without major isotope hypothesis

Manon Lincker, Jennifer Druhan, Sophie Guillon, Vincent Lagneau

# Thermodynamic and kinetic constants for isotopic fractionation modeling with or without major isotope hypothesis

Manon Lincker[a], Jennifer L. Druhan[b], Sophie Guillon[a], Vincent Lagneau[a]

[a] *Centre de Geosciences, MINES ParisTech, PSL Research University, Paris, FRANCE*
[b] *Department of Geology, University of Illinois Urbana Champaign, Urbana, IL, USA*

**Abstract**

The modeling capacities of geochemical speciation and reactive transport software continue to develop, and stable isotopes are now increasingly incorporated into these codes. Isotopic fractionation associated with a given chemical reaction is commonly modeled by affecting different *calculated* rate and thermodynamic constants for each explicitly defined isotopologue based on the classical thermodynamic constant of a reaction and the fractionation factor associated to the *modeled* reaction. This approach has been reliably demonstrated for cases in which one isotope is much more abundant (i.e. common) than the others (e.g. carbon, oxygen, nitrogen, etc.). Such large disparity in abundance allows the assumption that the thermodynamic constant of the isotopologue bearing the major isotope is essentially equal to the classical constant for the element. Kinetic rate constants for different isotopologues are also frequently determined by assuming that the rate of the reaction involving the major isotope is very close to the overall rate.

As our ability to accurately measure more isotopic systems expands, it becomes necessary to define the scope of validity of the rare isotope hypothesis and the errors introduced in application to elements like chlorine, bromine, zinc or others that do not present a clearly abundant major isotope. This study reviews the mathematical developments of thermodynamic and kinetic rate constant calculations following the major isotope hypothesis and expands upon this basis to provide appropriate thermodynamic parameterization where this assumption could introduce errors. The results show that the assumption brought by the major isotope hypothesis is also valid in isotopic systems without a major isotope for the determination of thermodynamic constants. This verification assures our ability to employ geochemical speciation codes to handle isotopic fractionation for a large variety of elements. The validity stems from the typically small deviations of relative concentrations and small differences in behavior for different isotopes. We illustrate these developments with an application case of zinc isotope fractionation modeling during sphalerite precipitation performed with the reactive transport code Hytec. The model scripts used for the application case are provided in this study and offer the opportunity for future benchmarking of software in application to explicit modeling of stable isotope fractionation.

*Keywords:* geochemical modeling, isotopic fractionation, major isotope hypothesis

## 1. Introduction

Geochemical speciation and reactive transport (RT) codes were originally developed several decades ago to provide a means of considering the long term implications and management of nuclear waste disposal [52], [77], [75]. Since then, these basic principles have been broadly expanded to other purposes like pollution remediation ([88], [87], [18], [5], [51]), mining [44], resources exploitation [71] and water-rock interactions [54].

Over a comparable period of time, stable isotope data have been increasingly utilized [80] for identification and quantification of water-rock interactions ([6], [7], [30], ...), weathering ( [17], [63], [47], [33], [37], ...), vegetation and rhizosphere cycling of water, soil or minerals ([12], [73], ...), pollution ([29], [15], [68], [60], [65], ...), contaminant degradation pathways such as chlorinated hydrocarbons ([90], [42], [41],...), oceanography ([35], [70], [3], [11], ...), paleoreconstruction ([50], [66], [78], [32], [31], ...) and biogeochemical cycling ([36], [39], [67], [19], [1], ...) .

RT software are now increasingly used to help interpret and fully leverage these isotopic data [27]. As isotopes and fractionating pathways continue to be incorporated and refined into reactive transport simulators ([25], [21], [24], [87], [89], [74], [22]) their capacity to allow a deeper and more quantitative understanding of reactive transformations and system dynamics is becoming increasingly evident.

Reactive transport models which explicitly include stable isotope fractionation have been developed for a variety of geoscience and environmental engineering applications including contamination( [87], [81], [82]), unsaturated zone water dynamics [72], flow and transport through heterogeneous porous media [23], experimental analogs ( [25], [21]), marine sediments pore fluids [55] and groundwater treatment systems [34], etc. These applications require a rigorous integration of isotopic and geochemical data for modeling purposes. Geochemical speciation codes are commonly based on the primary component or basis species approach [53], in which the total number of chemical species tracked during transport is limited to the number that are linearly independent from one another. Practically speaking, there is no need to waste computational effort tracking the advection of both bicarbonate and carbonic acid if they are coupled through an equilibrium relationship. Implementation of isotopic fractionation then means that each isotope must be created as a primary component, with all necessary attendant equilibria described. This exercise is usually performed by duplicating entries within the thermodynamic database, so that each isotopologue is considered as a fully-fledged chemical species ([27], [26], [87], [23], [24]).

Kinetically controlled reactions are modeled by reactive transport codes by defining the parameters of a selected kinetic law linking two or more components. When modeling kinetic isotopic fractionation, the common strategy is consistent with equilibrium reactions and involves duplication of isotopes as unique

*Corresponding author
*Email address:* manon.lincker@mines-paristech.fr (Manon Lincker)
[1]Present address: manon.lincker@live.com

'species' in the database so that they may be assigned different rate constants depending on the isotopologue involved in the reaction to reproduce kinetic isotopic fractionation.

This approach brings the significant advantage that the basic framework of the pre-existing RT codes remains unchanged, requiring only appropriate identification of parameter values. Typically, this is accomplished by reasonably assuming that the thermodynamic and/or rate constant used for the overall or 'bulk' formation of a given compound are effectively equivalent to those describing the most abundant isotope. For example, the equilibrium constant describing the abundance of bicarbonate and water through the dissociation of carbonic acid would be used to describe the $^{12}C$ isotopologue of these compounds. The thermodynamic or rate constants of the rarer isotope(s) (e.g. $^{13}C$) are then determined based on reported fractionation factors [27] appropriate for each equilibrium or kinetic reaction at a given temperature.

As the capacity for highly precise mass ratio measurements continues to expand, an increasing number of isotope systems are being developed in application to geosciences and environmental engineering studies. Unlike the 'traditional' isotope systems (e.g. H, C, N, O, S), many of these elements do not present a major isotope, for instance Cl [38], [41], Mo [58], [8], Br [69], Cu [45], [57], Zn [14], [62], etc. The issue of the major isotope was considered several decades ago by Thorstenson and Parkhurst [79] , who offered direct derivations of the individual isotope equilibrium constants of some species, e.g. $CO_{2(g)}$, $CO_{2(aq)}$, $HCO_3^-$, $CO_3^{2-}$, $CaCO_{3(aq)}$, $H_2O_{(g)}$, $H_2O_{(l)}$, $H_3O^+$, $OH^-$, $HCO_3^-$ and $CO_3^{2-}$ in ions pairs with $Na^+$, $K^+$, $Ca^{2+}$ and $Mg^{2+}$ following the earlier approach developed by Urey (1947) [80]. While the methodology does not require the definition of a major isotope, it cannot be readily generalized and requires an accounting of the degree of symmetry of exchanged atoms which the authors only provided for the aforementioned species [79]. Therefore, continued expansion of isotope-enabled RT applications suggests that the common method by which isotopic partitioning is implemented in these models requires careful consideration, and, where necessary, a more generalized approach such that the benefits of RT codes can be applied to emerging isotopic compounds that do not have an obvious choice of major isotope.

The present study addresses this need by revisiting the classical mathematical formulation for equilibrium and kinetic isotopic fractionation as typically implemented in RT codes to produce a generalized method relaxing the constraint associated with the need for a major isotope. We will first walk through a series of modifications to the formal approach of equilibrium fractionation, then consider the extension to kinetic fractionation and finally offer a demonstration in the context of zinc isotopes in Mississippi Valley Type (MVT) ore deposits.

## 2. Classical method for equilibrium isotopic fractionation modeling with RT codes

Reactive transport codes developed following the basis species approach [53] consider isotopologues as individual components with their own thermodynamic constants. This means that two isotopes of a given element in a given compound exist as two separate 'species' that operate in tandem through parallel reactions

and transport pathways. One of the most basic ways in which these 'species' are tied together as isotopes of the same element is through the slight differences in their thermodynamic constants, which stems from mass-dependent equilibrium fractionation. We begin with the mathematical development commonly used to determine the thermodynamic constants for reactions involving different isotopologues.

### *2.1. Duplication of isotopologues in the database*

In the following equations, $E_i$ stands for a basis species (mol.kg$^{-1}$), $\bar{E}$ for a derived species (mol.kg$^{-1}$), $\gamma$ for the activity coefficient, $N_c$ is the number of basis components and $\nu$ represents the stoichiometric coefficients. We hereby present the general formalism, which is appropriate to any isotope system of interest. For the sake of clarity, we also offer an example: isotopes of sulfur in anhydrite and sulfates (where $^{32}$S can be considered as a major isotope and $^{34}$S as a minor isotope of sulfur). Critically, this choice is intended only for the sake of clarity and does not restrict the derivation to this context.

Let us consider the following chemical reaction :

$$\sum_{i=0}^{N_c-1} \nu_i E_i \rightleftharpoons \bar{E}, \tag{1}$$

and its associated equilibrium constant:

$$K = \frac{\bar{\gamma} \cdot \bar{E}}{\prod_i \gamma_i^{\nu_i} E_i^{\nu_i}} \tag{2}$$

For the specific case of $CaSO_4$ formation, it becomes :

$$\mathrm{Ca}^{2+} + \mathrm{SO}_4^{2-} \rightleftharpoons \mathrm{CaSO}_{4(s)}, \tag{3}$$

$$K_{\mathrm{CaSO}_{4(s)}} = \frac{\gamma_{\mathrm{CaSO}_{4(s)}} \mathrm{CaSO}_{4(s)}}{\gamma_{\mathrm{Ca}^{2+}} \mathrm{Ca}^{2+} \cdot \gamma_{\mathrm{SO}_4^{2-}} \mathrm{SO}_4^{2-}}. \tag{4}$$

When multiple isotopes of one element are considered, they are denoted through an isotope index $\lambda$. For example, $E^0$ and $E^\lambda$ or for our particular case study $^{32}S$ and $^{34}S$. We represent $E_0$ as the basis species which carries the isotopes, namely $SO_4^{2-}$ for the $S$ isotopes example. In equation (1), this carrying species is isolated out of the sum leading to:

$$\nu_0 E_0 + \sum_{i=1}^{N_c-1} \nu_i E_i \rightleftharpoons \bar{E} \tag{5}$$

Let us assume only two isotopes for the moment: the major (most abundant one, *e.g.* $^{32}$S) and a minor one (least abundant, *e.g.* $^{34}$S). Furthermore, let us assume here that there is only one isotopically substituted element in the derived species. $E_0^0$ is substituted only once by $E_0^\lambda$ in $\bar{E^\lambda}$:

$$(\nu_0 - 1)E_0^0 + E_0^\lambda + \sum_{i=1}^{N_c-1} \nu_i E_i \rightleftharpoons \bar{E^\lambda}. \tag{6}$$

The equilibrium constant can be written as:

$$K = \frac{\bar{\gamma}\bar{E^{\lambda}}}{\gamma_0^{\nu_0}(E_0^{0(\nu_0-1)} \cdot E_0^{\lambda}) \cdot \prod_{i=1}^{N_c-1} \gamma_i^{\nu_i} E_i^{\nu_i}}, \tag{7}$$

In the case of our example, only one atom of sulfur is considered, thus the stoichiometry of $SO_4^{2-}$ is 1 ($\nu_0 = 1$). We introduce $N_{iso}$ the number of different isotopes considered and the isotopic ratios $R^{\lambda} = \bar{E}^{\lambda}/\bar{E}^{0}$ and $R_0^{\lambda} = \bar{E}_0^{\lambda}/\bar{E}_0^{0}$. Substituting $R^{\lambda}$ and $R_0^{\lambda}$ in (2) isolates the thermodynamic constant of the major isotope:

$$K = K^0 \frac{\left(1 + \sum_{\lambda=1}^{N_{\text{iso}}-1} R^{\lambda}\right)}{\left(1 + \sum_{\lambda=1}^{N_{\text{iso}}-1} R_0^{\lambda}\right)^{\nu_0}}. \tag{8}$$

Likewise for the $CaSO_{4(s)}$ example:

$$K = K^{32} \frac{\left(1 + R^{34}_{\text{CaSO}_{4(s)}}\right)}{\left(1 + R^{34}_{\text{SO}_4^{2-}}\right)} \tag{9}$$

### *2.2. Simplification based on major isotope hypothesis*

Where the major isotope assumption holds true, the isotopic ratios are very small (compared to 1) and it is reasonable to assume that the thermodynamic constant $K$ of the major isotope ($K^{32}$ in our example) equals the generally known constant for the bulk chemical species, as is often already available in geochemical databases. Physically, this leads to the assumption that there is one isotope whose abundance is predominant compared to others. This assumption, which is valid for many elements (like C, N, O, Ca, K, S, Fe, Li, ...), yields a condition under which $R^{\lambda} << 1$ and $R_0^{\lambda} << 1$ so that $\sum_{\lambda} R^{\lambda} << 1$ and $\sum_{\lambda} R_0^{\lambda} << 1$. As a consequence, :

$$K^0 \simeq K \tag{10}$$

For our $CaSO_{4(s)}$ example, we can safely assume that $R^{34}_{\text{CaSO}_{4(s)}} << 1$ and $R^{34}_{\text{SO}_4^{2-}} << 1$. This leads to

$$K^{32} \simeq K \tag{11}$$

The equilibrium fractionation factor is defined as follows:

$$\alpha^{\lambda}_{B-A} = \frac{R^{\lambda}_B}{R^{\lambda}_A} \tag{12}$$

with $A$ standing for the reactant, $B$ for the instantaneous product and $\lambda$ the isotope. Using the fractionation factor between two species, the equilibrium constant for the reaction which involves a minor isotope can be written as a function of the equilibrium constant of the major isotope reaction :

$$\alpha_0^\lambda = \frac{R^\lambda}{R_0^\lambda} = \frac{\frac{\bar{E^\lambda}}{\bar{E^0}}}{\frac{E_0^\lambda}{E_0^0}} = \frac{K^\lambda}{K^0} \tag{13}$$

so that

$$K^\lambda \simeq \alpha_0^\lambda K. \tag{14}$$

Continuing with $CaSO_4$ example:

$$\alpha^{34}_{\mathrm{CaSO}_{4(s)}-\mathrm{SO}_4^{2-}} = \frac{K^{34}}{K^{32}} \tag{15}$$

and

$$K^{34} \simeq \alpha^{34}_{\mathrm{CaSO}_{4(s)}-\mathrm{SO}_4^{2-}} \cdot K \tag{16}$$

### *2.3. Limitations*

We now expand our consideration to the potential for error introduced when such an approach is applied to elements without significant difference in abundance(s) between the major and minor isotope(s) (Ni, Cu, Zn, Mg, Cl, Br, etc). These concerns motivate a generalization of the calculations described above for thermodynamic constants without the need to invoke a major isotope hypothesis.

## 3. Calculation: Circumvention of the major isotope hypothesis

### *3.1. Simple substitution*

Here we propose to expand the calculations described above to avoid the use of the major isotope assumption. Instead of the major isotope hypothesis, we rely on characteristically small variations of enrichment factor $\epsilon$ (defined as $1-\alpha$) and $\epsilon R$. As a secure upper limit of enrichment in natural systems, we can assume that $\epsilon$ is smaller than 100‰ (*i.e.* $\alpha$ between 0.90 and 1.1). This is generally a safe assumption for the $\epsilon$ values of low- (e.g. C, N) and mid-mass (e.g. Ca) isotope systems [59], [9], [61], [13], [26] and even holds true for large differences in mass among the isotopes of a given element, as in the case of Li [10]. In the following mathematical developments, the second order and higher terms in $\epsilon R$ will therefore be neglected.

Once again we consider the following reaction where element $E_0$ has two isotopologues $E_0^0$ and $E_0^\lambda$:

$$E_0 + \sum_{i=1}^{N_c-1} \nu_i E_i \rightleftharpoons \bar{E}. \tag{17}$$

Therefore, we can define the following isotopic ratios $R$, fractionation factor $\alpha$ and enrichment factor $\epsilon$:

$$R_0^\lambda = \frac{E_0^\lambda}{E_0^0} \tag{18}$$

$$\bar{R}^\lambda = \frac{\bar{E}^\lambda}{\bar{E}^0} \tag{19}$$

$$\alpha^\lambda = \frac{\bar{R}^\lambda}{R_0^\lambda} = 1 - \epsilon^\lambda. \tag{20}$$

The derivation of equilibrium constant $K$ leads to:

$$K = \frac{\bar{\gamma}\bar{E}}{\gamma_0 E_0 \cdot \prod_i (\gamma_i E_i)^{\nu_i}} = \frac{\bar{\gamma}\bar{E}^0 \cdot \left(1 + \frac{\bar{E}^\lambda}{\bar{E}^0}\right)}{\gamma_0 E_0 \cdot \prod_i (\gamma_i E_i)^{\nu_i} \cdot \left(1 + \frac{E_0^\lambda}{E_0^0}\right)} = K^0 \cdot \frac{1 + \alpha^\lambda R_0^\lambda}{1 + R_0^\lambda} = K^0 \cdot \frac{1 + R_0^\lambda + \epsilon^\lambda R_0^\lambda}{1 + R_0^\lambda} \tag{21}$$

where $K^0$ is the equilibrium constant of the reaction involving $E_0^0$ as $E_0$ isotopologue.

Thus

$$K^0 = K \cdot \frac{1 + R_0^\lambda}{1 + R_0^\lambda + \epsilon^\lambda R_0^\lambda} \tag{22}$$

and

$$K^\lambda = \alpha^\lambda \cdot K \cdot \frac{1 + R_0^\lambda}{1 + R_0^\lambda + \epsilon^\lambda R_0^\lambda}. \tag{23}$$

In the specific case where $E_0^0$ is a *major* isotope, this result is identical to section 2.

We call now $T_0$ the total of species $E_0$ such as $T_0 = \bar{E} + E_0$. Using the equilibrium constant $K$ to express $E_0$ leads to:

$$E_0 = \frac{T_0}{1 + K\frac{\gamma_0}{\bar{\gamma}} \prod_i (\gamma_i E_i)^{\nu_i}}. \tag{24}$$

We next investigate the difference in accuracy when using the simplification derived from the major isotope hypothesis but without making any assumption about the relative abundance of any isotopologues. For this purpose, we will use the precise expression of the equilibrium constants of the reactions involving isotopologues $E_0^0$ and $E_0^\lambda$ respectively (equations 22 and 23) and approximation of these constants: $K^0 = K$ and $K^\lambda = \alpha^\lambda K$, corresponding to equations 10 and 14. To evaluate these approximations we monitor the isotopic ratio $\hat{R}_0^\lambda$ when using approximations relative to the isotopic ratio $R_0^\lambda$ when using exact equilibrium constants (equations 22, 23). This leads to:

$$
\begin{aligned}
\mathrm{R} = \frac{\hat{R}_0^\lambda}{R_0^\lambda} = \frac{\frac{\hat{E}_0^\lambda}{\hat{E}_0^0}}{\frac{E_0^\lambda}{E_0^0}} &= \frac{\frac{1+K\frac{\gamma_0}{\bar{\gamma}}\prod_i(\gamma_i E_i)^{\nu_i}}{T_0^0}\cdot\frac{T_0^\lambda}{1+\alpha^\lambda K\frac{\gamma_0}{\bar{\gamma}}\prod_i(\gamma_i E_i)^{\nu_i}}}{\frac{1+K^0\frac{\gamma_0}{\bar{\gamma}}\prod_i(\gamma_i E_i)^{\nu_i}}{T_0^0}\cdot\frac{T_0^\lambda}{1+K^\lambda\frac{\gamma_0}{\bar{\gamma}}\prod_i(\gamma_i E_i)^{\nu_i}}} \\
&= \frac{1+K^0\frac{\gamma_0}{\bar{\gamma}}\prod_i(\gamma_i E_i)^{\nu_i}}{1+K\frac{\gamma_0}{\bar{\gamma}}\prod_i(\gamma_i E_i)^{\nu_i}}\cdot\frac{1+\alpha^\lambda K\frac{\gamma_0}{\bar{\gamma}}\prod_i(\gamma_i E_i)^{\nu_i}}{1+K^\lambda\frac{\gamma_0}{\bar{\gamma}}\prod_i(\gamma_i E_i)^{\nu_i}} \\
&= \frac{1+K^0 Z}{1+KZ}\cdot\frac{1+\alpha^\lambda KZ}{1+K^\lambda Z}
\end{aligned}
\tag{25}
$$

where $Z = \frac{\gamma_0}{\bar{\gamma}}\prod_i(\gamma_i E_i)^{\nu_i}$.

Using Taylor expansion on equations 22 and 23:

$$
K^0 = K\left(1+\frac{\epsilon^\lambda R_0^\lambda}{1+R}+\mathrm{o}\left(\left(\epsilon^\lambda R\right)^2\right)\right) \tag{26}
$$

and

$$
K^\lambda = \alpha^\lambda K\left(1+\frac{\epsilon^\lambda R_0^\lambda}{1+R}+\mathrm{o}\left(\epsilon^\lambda R\right)^2\right). \tag{27}
$$

Then, incorporating 26 and 27 in 25:

$$
\mathrm{R} = \frac{1+KZ\left(1+\alpha^\lambda\right)+KZ\left(\frac{\epsilon^\lambda R_0^\lambda}{1+R_0^\lambda}\right)+\alpha^\lambda K^2Z^2\left(1+\frac{\epsilon^\lambda R_0^\lambda}{1+R_0^\lambda}\right)}{1+KZ\left(1+\alpha^\lambda\right)+\alpha^\lambda KZ\left(\frac{\epsilon^\lambda R_0^\lambda}{1+R_0^\lambda}\right)+\alpha^\lambda K^2Z^2\left(1+\frac{\epsilon^\lambda R_0^\lambda}{1+R_0^\lambda}\right)}. \tag{28}
$$

However,

$$
\alpha^\lambda KZ\frac{\epsilon^\lambda R_0^\lambda}{1+R_0^\lambda} = \left(1-\epsilon^\lambda\right)KZ\frac{\epsilon^\lambda R_0^\lambda}{1+R_0^\lambda} = KZ\frac{\epsilon^\lambda R_0^\lambda}{1+R_0^\lambda}+\mathrm{o}\left(\epsilon^\lambda R_0^\lambda\right)^2, \tag{29}
$$

and thus,

$$
\mathrm{R} = 1+\mathrm{o}\left(\epsilon^\lambda R_0^\lambda\right)^2. \tag{30}
$$

This result shows that the error introduced by using the approximation is of the order $\mathrm{o}\left(\epsilon^\lambda R_0^\lambda\right)^2$.

### 3.2. Limitations

Results show that the error on the isotopic ratio deriving from the use of the approximation $K^0 = K$ and $K^\lambda = \alpha K$ is in the order of $(\epsilon R)^2$. With $\epsilon$ usually less (or much less) than 0.1, the assumption on thermodynamic constant can be safely in most natural applications. The ultra-major isotope has already been presented (see subsection *Simplification based on major isotope hypothesis*). For less discriminating isotopic ratios, we stressed that the choice of reference isotope was arbitrary; therefore, when one isotope has a clearly higher relative abundance than the other, the smartest choice is to choose it as a reference (with resulting $R < 1$, the error is further reduced). This still holds true for isotopes of similar concentrations, with $R \simeq 1$. In all cases, it is probably safer to check whether $\epsilon R$ is indeed small enough for the acceptable error. Finally, only one application might lead to unacceptable errors: when the most abundant isotope changes over time or space in the same system (e.g. $R \simeq 0.2$ to 0.8), and for larger values of $\epsilon$, although the authors cannot imagine natural cases falling into these conditions.

### 3.3. Extension to double substitution

We next extend this methodology to address the case of double substitution. We consider here the following reaction:

$$E_0 + E_1 + \sum_{i=2}^{Nc-2} \nu_i E_i \rightleftharpoons \bar{E} \tag{31}$$

where $E_0$ and $E_1$ have two possible isotopes (0 and $\lambda$).

We suppose that:

$$\bar{R}^{\lambda\star} = \frac{\bar{E}^{\lambda\star}}{\bar{E}^{0\star}} = \frac{\bar{E}^{\lambda 0}}{\bar{E}^{00}} = \frac{\bar{E}^{\lambda\lambda}}{\bar{E}^{0\lambda}} \tag{32}$$

and

$$\bar{R}^{\star\lambda} = \frac{\bar{E}^{\star\lambda}}{\bar{E}^{\star 0}} = \frac{\bar{E}^{0\lambda}}{\bar{E}^{00}} = \frac{\bar{E}^{\lambda\lambda}}{\bar{E}^{\lambda 0}}. \tag{33}$$

As for the case of one element bringing isotopes in the reaction, activity coefficients and $E_i$ terms will be removed from the calculation of the ratio as they will be divided by themselves.

The equilibrium constant can be written as:

$$K = \frac{\bar{E}^{00} + \bar{E}^{0\lambda} + \bar{E}^{\lambda 0} + \bar{E}^{\lambda\lambda}}{\left(E_0^0 + E_0^\lambda\right)\left(E_1^0 + E_1^\lambda\right)}. \tag{34}$$

We can then derive the specific equilibrium constants:

$$K = K^{00}\frac{1 + \bar{R}^{\star\lambda} + \bar{R}^{\lambda\star} + \bar{R}^{\star\lambda}\bar{R}^{\lambda\star}}{\left(1 + R_0^\lambda\right)\left(1 + R_1^\lambda\right)} \tag{35}$$

where $R_0^\lambda = \frac{E_0^\lambda}{E_0^0}$ and $R_1^\lambda = \frac{E_1^\lambda}{E_1^0}$.

Thus,

$$K^{00} = K\frac{\left(1+R_0^\lambda\right)\left(1+R_1^\lambda\right)}{1+\alpha_0^\lambda R_0^\lambda + \alpha_1^\lambda R_1^\lambda + \alpha_0^\lambda\alpha_1^\lambda R_0^\lambda R_1^\lambda}. \tag{36}$$

Using the same methodology, it appears that:

$$K^{\lambda 0} = \alpha_0^\lambda \cdot K\frac{\left(1+R_0^\lambda\right)\left(1+R_1^\lambda\right)}{1+\alpha_0^\lambda R_0^\lambda + \alpha_1^\lambda R_1^\lambda + \alpha_0^\lambda\alpha_1^\lambda R_0^\lambda R_1^\lambda}. \tag{37}$$

We will now focus on $E_0$ and its isotopes, assuming that the $E_1$ isotopologue involved in the reaction is $E_1^0$. We can write the following reactions:

$$E_0^0 + E_1^0 \rightleftharpoons \bar{E}^{00} \tag{38}$$

$$E_0^\lambda + E_1^0 \rightleftharpoons \bar{E}^{\lambda 0}. \tag{39}$$

Considering $T_0^0$ the total of species $E_0^0$ and $T_0^\lambda$ the total of species $E_0^\lambda$:

$$E_0^0 = \frac{T_0^0}{1+K^{00}E_1^0} \tag{40}$$

$$E_0^\lambda = \frac{T_0^\lambda}{1+K^{\lambda 0}E_1^0}. \tag{41}$$

As for the case of one species bringing isotopes in the system, we track the relative difference in the isotopic ratio when using $K$ and $\alpha_0^\lambda$ for approximation relative to the isotopic ratio when using constants $K^{00}$ and $K^{\lambda 0}$.

$$\begin{aligned} \mathrm{R} &= \frac{R_0^\lambda}{\hat{R}_0^\lambda} = \frac{\frac{E_0^\lambda}{E_0^0}}{\frac{\hat{E}_0^\lambda}{\hat{E}_0^0}} = \frac{1+K^{00}E_1^0}{1+K^{\lambda 0}E_0^\lambda}\cdot\frac{1+\alpha_0^\lambda K E_1^0}{1+KE_1^0} \\ &= \frac{1+E_1^0 K\dfrac{\left(1+R_0^\lambda\right)\left(1+R_1^\lambda\right)}{1+\alpha_0^\lambda R_0^\lambda + \alpha_1^\lambda R_1^\lambda + \alpha_0^\lambda\alpha_1^\lambda R_0^\lambda R_1^\lambda}}{1+\alpha_0^\lambda E_1^0 K\dfrac{\left(1+R_0^\lambda\right)\left(1+R_1^\lambda\right)}{1+\alpha_0^\lambda R_0^\lambda + \alpha_1^\lambda R_1^\lambda + \alpha_0^\lambda\alpha_1^\lambda R_0^\lambda R_1^\lambda}}\cdot\frac{1+\alpha_0^\lambda K E_1^0}{1+KE_1^0}. \end{aligned} \tag{42}$$

Noting that

$$\frac{1+\alpha_0^\lambda R_0^\lambda + \alpha_1^\lambda R_1^\lambda + \alpha_0^\lambda\alpha_1^\lambda R_0^\lambda R_1^\lambda}{\left(1+R_0^\lambda\right)\left(1+R_1^\lambda\right)} = 1 - \frac{\epsilon_0^\lambda R_0^\lambda\left(1+R_1^\lambda\right) + \epsilon_1^\lambda R_1^\lambda\left(1+R_0^\lambda\right)}{\left(1+R_0^\lambda\right)\left(1+R_1^\lambda\right)} + \mathrm{o}\left(\epsilon_0^\lambda\epsilon_1^\lambda R_0^\lambda R_1^\lambda\right) \tag{43}$$

it follows that

$$\mathrm{R} = 1 + \mathrm{o}\left(\epsilon_0^\lambda\epsilon_1^\lambda R_0^\lambda R_1^\lambda\right). \tag{44}$$

This result is comparable to equation 30 and shows that the error induced by using the bulk thermodynamic constant and the fractionation factor instead of isotopes specific thermodynamic constants is negligible. This assumption can then be safely used.

## 4. Calculation: Developments for kinetic rate constant calculation

Next we turn to a comparable calculation for kinetically regulated reactions. The formalism for kinetic reactions is consistent with that developed and used by [46], [76], [20], [26].

Starting with the formation of a species $\bar{E}$ with two isotopes comprising species $E_0$ ($E_0^0$ and $E_0^\lambda$)

$$E_0 + \sum_{i=1}^{N_c-1} \nu_i E_i \rightarrow \bar{E} \tag{45}$$

we can defined the rate ${}^+V$ of both reactions involving the different isotopologues

$${}^+V^0 =^+ k^0 a_0^0 \prod_{i=1}^{Nc-1} a_i^{\nu_i} \tag{46}$$

$${}^+V^\lambda =^+ k^\lambda a_0^\lambda \prod_{i=1}^{Nc-1} a_i^{\nu_i}. \tag{47}$$

The global rate of the bulk reaction is then defined by

$${}^+V \quad = \quad {}^+ka_0 \cdot \prod_{i=1}^{Nc-1} a_i^{\nu_i} =^+ V^0 +^+ V^\lambda \tag{48}$$

Similarly to the thermodynamic developments, we investigate here the ratio of the exact global rate over the approximated rate:

$$\mathrm{R} = \frac{{}^+\hat{V}}{{}^+V} = \frac{k^0 a_0^0 + k^\lambda a_0^\lambda}{k\left(a_0^0 + \alpha^\lambda a_0^\lambda\right)} = \frac{k^0\left(a_0^0 + \alpha^\lambda a_0^\lambda\right)}{k\left(a_0^0 + \alpha^\lambda a_0^\lambda\right)} = \frac{k^0}{k}. \tag{49}$$

From equation 48 it follows that:

$$ka_0 = k^0 a_0^0 + \alpha^\lambda k^0 a_0^\lambda = k^0\left(a_0^0 + a_0^\lambda - \epsilon^\lambda a_0^\lambda\right) \tag{50}$$

and thus

$$\frac{k^0}{k} = \frac{a_0^0 + a_0^\lambda}{a_0^0 + a_0^\lambda - \epsilon^\lambda a_0^\lambda} = \frac{1}{1 - \dfrac{\epsilon a_0^\lambda}{a_0^0 + a_0^\lambda}}. \tag{51}$$

Using Taylor expansion:

$$\frac{k^0}{k} = 1 + \frac{\epsilon a_0^\lambda}{a_0} + \mathrm{o}\left(\frac{\epsilon^\lambda a_0^\lambda}{a_0}\right)^2 = 1 + \frac{\epsilon^\lambda R^\lambda}{1 + R^\lambda} + \mathrm{o}\left(\frac{\epsilon^\lambda R^\lambda}{1 + R^\lambda}\right)^2 \tag{52}$$

where R stands for the isotopic ratio. We note that in the case of a kinetic reaction forming or dissolving a mineral, one may wish to develop the expressions shown above as a 'forward' reaction and track overall mineral growth or dissolution as the net rate arising from the difference between this reaction and a 'backward' reaction proceeding in the opposite direction. The same development can be done for the backward reaction and thus these unidirectional pathways can be combined into a net rate and applied to the common class of fractionating reactions associated with mineral growth and solubilization.

## 5. Discussion

The above derivations extend the validity of equations with isotopic fractionation which can be found in certain reactive transport codes, without the need for the major isotope assumption in the case of thermodynamic equilibrium. These mathematical developments are not exhaustive, but they expand the capacity to handle isotopic fractionation modeling for a large variety of chemical species. These developments show that no *a priori* assumption is required for the relative isotopic abundances. Instead, the ratios may be defined relative to an arbitrary choice of reference isotope. The possible deviation from the exact solution is introduced through assumptions regarding the (small) magnitude of enrichment factors. In natural systems these distributions are usually narrow, and thus this assumption improves upon the prior approach in which the presence of a major isotope in a given element was required. When neglecting terms in $(\epsilon R)^2$, the equations correspond to the ones obtained using the major isotope hypothesis and the classical approach.

The derivations for kinetically controlled reactions such as mineral precipitation and dissolution show that the error introduced when using $k$ and $\alpha^{\lambda}k$ instead of $k^0$ and $k^{\lambda}$ depends on $R$, which changes over time during the progress of the reaction. This issue has been considered in prior studies, largely in the context of organic contaminants [43], [83]. A solution was offered using a probability term which is a function of the abundance of the heavy and light isotopes through the course of the reaction, the number of atoms possibly isotopically substituted in the molecule and number of reactive positions among them (described as the 'isotopologues approach' in [43]). The reaction rates resulting from this approach are distinct from the bulk rate, such that the light isotope reacts slightly faster, and the heavy isotope slightly slower than what would be the bulk rate. The average rate weighted by the probability of the presence of a heavy isotope then reproduces the bulk rate.

Here, in absence of specific experimentally determined rate constants for the isotopologues, we offer a generalized demonstration that assuming the rate of one isotopologue is comparable to the bulk rate constants and deriving the other rate constants using the fractionation factor is a reasonable approximation when dealing with elements which present a clear major isotope (isotopic ratio $R$ is then small). The error introduced by this approximation may become problematic when dealing with elements with isotopes of comparable relative abundance, and thus the use of a correction term as detailed in [43] and [83] could become warranted. We provide a framework to evaluate the magnitude of these errors in application to

kinetic rate expressions, and extend consideration of these assumptions to applications beyond organic contaminants, such as mineral precipitation and dissolution. These developments are provided with the intent of raising awareness among the reactive transport community about the potential errors introduced when modeling fractionation of isotopes lacking a clear major abundance, which have thus far largely been limited to the specific context of aqueous chlorinated compounds.

As analytical capabilities increasingly enable determination of the specific location of substituted atoms within a molecular structure ([16], [40], [64]), it remains to be shown whether such an approach will facilitate treatment of the complexity of partitioning coefficients in natural systems.

## 6. Application case study

As an illustrative example of the utility of the previous sections, we provide an application of geochemical modeling including equilibrium isotopic fractionation. Two simulations were performed with the CHESS speciation code [85], [84] and are inspired by the distribution of zinc isotopes (no major isotope) within Mississippi Valley Type (MVT) ore deposits. In this system, zinc isotopic signatures have been shown to differentiate depending upon the history of the deposit. MVT ore formation is characterized by the combination of hydrothermal systems and major crustal tectonic events [49], [4]. The precipitation of the ore is related to fluid migration and more specifically to dense basinal brines with temperatures between 75 and 200C, typically in carbonated platforms [49]. MVT ores gather a large variety of deposits and some aspects are still debated, including the origin of the ore fluids, the timescale of fluid migration and the processes of precipitation. Despite this uncertainty, prior studies have shown that a plausible condition for ore formation involves mixing between hot fluids containing elevated metal concentrations and cooler fluids with high reduced sulfur content [48]. This overly simplified illustrative case can be linked to the second part of section 3 about double substitution, namely 2 isotopes of a single Zn atom in $Zn^{2+}$ and ZnS compounds, with comparable abundances for the two Zn isotopes. The two simulations illustrate equilibrium and kinetic fractionation respectively.

*Equilibrium fractionation.* We provide a simplified simulation of a progressive mixing of two (sulfide bearing and zinc bearing) solutions leading to sphalerite precipitation with associated zinc isotopes fractionation. The simulation consists of a sequential addition of a constant volume (0.002 L per sample, 100 samples) of solution 2 into solution 1 (table 1). The cumulative volume of the mixed solution is denoted as $\zeta$. We illustrate here that isotopic enrichment at equilibrium can be simulated through the definition of appropriate thermodynamic constants. In this model, we focus on the isotopic composition of the mineral sphalerite. To this purpose, sphalerite was considered as a solid solution. This approach allows us to define different endmembers of pure $^{64}$Zn or $^{66}$Zn sphalerite and all intermediate compositions. As the ratio $\frac{^{66}\mathrm{Zn}}{^{64}\mathrm{Zn}}$ is close

Table 1: Simulation parameters (balance means that it was adjusted to ensure solution electroneutrality)

| | solution 1 | solution 2 |
|---|---|---|
| volume (L) | 1 | 0.2 |
| temperature (C) | 60 | 150 |
| dolomite (mol/L) | 1 | 0 |
| $^{64}Zn^{2+}$ (mol/L) | 6.33081e-03 | 0 |
| $^{66}Zn^{2+}$ (mol/L) | 3.66919e-03 | 0 |
| $Cl^-$ (mol/L) | balance | 0 |
| $H_2S$ (mol/L) | 0 | 1e-02 |
| $Na^+$ (mol/L) | 0 | balance |
| $CO_2$ fugacity (atm) | 1 | 60 |
| pH | equilibrium (5.87) | 4.2 |

to 0.5, using the major isotope hypothesis to assume that $^{64}K_{Sphalerite}$=$K_{Sphalerite}$ seems hazardous. But the developments detailed in this study showed that this assumption can indeed be performed safely.

Initial concentrations of $^{64}Zn^{2+}$ and $^{66}Zn^{2+}$ were calculated in order to produce a cumulative concentration of $1 \times 10^{-2}$ mol/L with the following parameters : a constant fractionation factor $\alpha_{eq}$=0.9997 (corresponding to the fractionation during sphalerite precipitation from $ZnSO_4$) was selected [86]. We refer here to an equilibrium fractionation factor in order to illustrate the previous developments, even if using an example of mineral precipitation. The same example is used later to illustrate the kinetic developments (with a TST rate law, which is usually used for kinetically-mediated mineral growth). Due to the lack of data, no dependence of the fractionation factor to the temperature is taken into account here. Initial $\delta^{66}Zn$ was set at 0‰ (arbitrarily chosen, $\delta^{66}Zn$ of terrestrial geological materials are within a range of -0.80 ‰ and 2.5 ‰ [28]) and the standard isotopic ratio $\frac{^{66}Zn}{^{64}Zn}$ was set to 0.56502 [56].

$$Zn^{2+} + H_2S \rightleftharpoons ZnS + 2H^+ \tag{53}$$

All thermodynamic constants K for sphalerite precipitation (53) were calculated using equations (10) to (14) at appropriate temperatures (table 2) following the methodology described in this study.

During the course of the simulation, pH decreases from 5.87 to 5.29 (figure 1a) and temperature increases from 60 to 75°C from pure solution 1 to a mixing ratio (figure 1b). $Zn^{2+}$ decreases of $2 \times 10^{-3}$ mol in stoichiometric agreement with sphalerite precipitation (figure 1c). Evolution of $\delta^{66}Zn$ in both zinc and sphalerite shows that the implemented thermodynamic constants accurately reproduce the reported enrichment of -0.3‰ during precipitation of sphalerite (figure 1d).

Table 2: Thermodynamic constants of sphalerite precipitation

| Temperature (C) | log K Sphalerite $^{64}$Zn | log K Sphalerite $^{66}$Zn |
|---|---|---|
| 0 | 4.632700000 | 4.632569692 |
| 25 | 4.452300000 | 4.452169692 |
| 60 | 4.185100000 | 4.184969692 |
| 100 | 3.876800000 | 3.876669692 |
| 150 | 3.51200000 | 3.5111869692 |
| 200 | 3.190400000 | 3.190269692 |
| 250 | 2.928600000 | 2.928469692 |
| 300 | 2.740400000 | 2.740269692 |

*Kinetic fractionation.* We also provide an example of fractionation modeling during kinetically controlled reaction. The same system was used with the difference that precipitation of sphalerite is kinetically constrained. The simulation was created without comparison to actual experimental results: its main purpose is to illustrate appropriate behavior isotopic fractionation during kinetically controlled reactions where a major isotope is lacking. The law and parameters determined by [2] were used to derive the kinetic rate constant for sphalerite precipitation at 70°C: $+5.04848 \times 10^{-12}$ mol/m$^2$/s in precipitation for $^{64}$Zn. Then we calculated the rate constant for $^{66}$Zn using the same fractionation factor than for the equilibrium precipitation case (0.9997), leading to a rate of $+5.046965456 \times 10^{-12}$ mol/m$^2$/s. The model simulates an initial solution oversaturated in zinc at 70°C and advances through time-dependent sphalerite formation over a duration of 1 hour (figure 2). At the end of the simulation, the solution is still over-saturated with respect to sphalerite.

The simulation results show that sphalerite precipitates faster at the beginning, when the conditions are the farthest from equilibrium (figure 2a). The precipitation rate decreases as the conditions get closer to equilibrium. The $\delta^{66}$Zn values show that sphalerite isotopic composition reaches the initial composition of aqueous $Zn^{2+}$ (i.e 0‰) rapidly (as sphalerite precipitates rapidly in early time) and remains below the values of aqueous $\delta^{66}$Zn (figure 2b). In the aqueous phase, $\delta^{66}$Zn increases rapidly due to the fast precipitation rate, and this kinetic fractionation persists as the solution is still over-satured with respect to sphalerite. By the end of the simulation, the rate has become reduced due to convergence to equilibrium conditions. The evolution of $\delta^{66}$Zn in the aqueous phase gives information about the $\delta^{66}$Zn of the incremental precipitating Zn (with a -0.3‰ enrichment) but the $\delta^{66}$Zn in the solid phase is an accumulated averaged, such that the sphalerite isotopic signature evolves mainly at the beginning of the simulation.

It is worthwhile to recall that in these CHESS simulations, as in most speciation and RT codes, the two isotopes of Zn are entered as unique 'species' with individual constants. The kinetic reaction driving sphalerite formation couples these two 'species' through the solid solution, and thus one may nominally sum up the concentration of $Zn^{64}$ and $Zn^{66}$ at any point in the simulation to retrieve a 'bulk' Zn concentration.

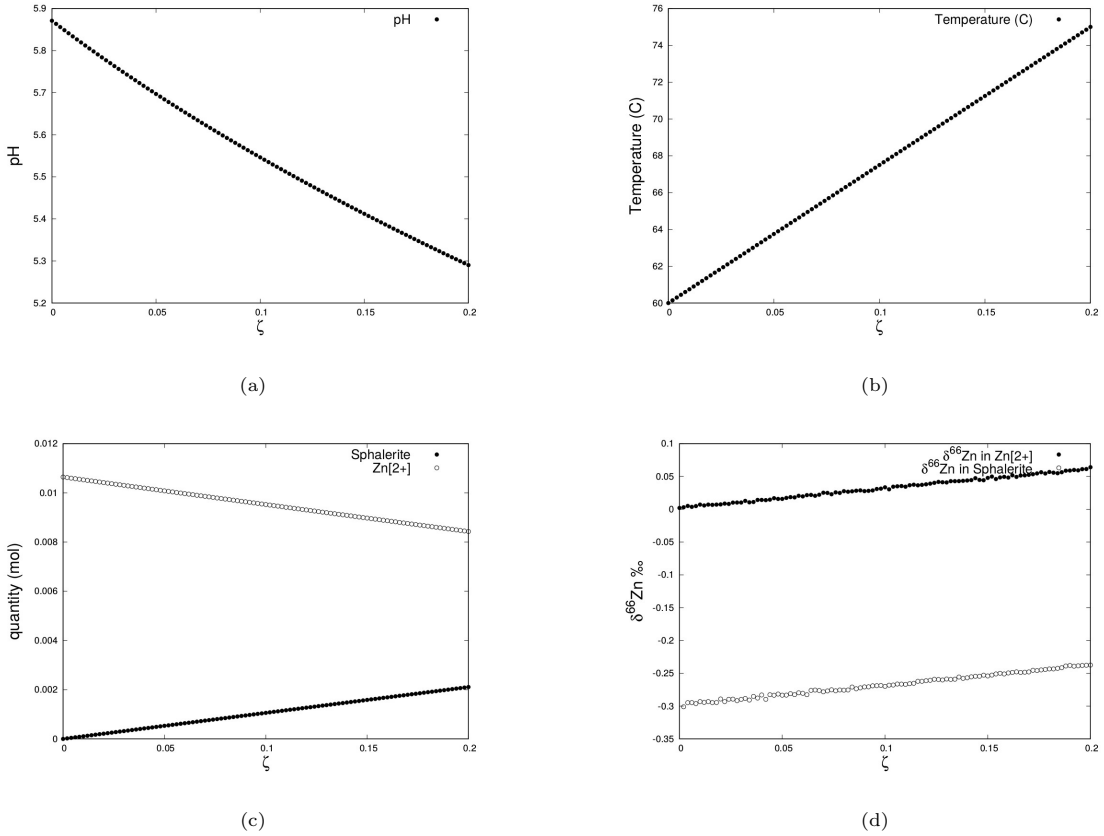


Figure 1: Simulation results during mixing: a. pH, b. temperature evolution, c. zinc and sphalerite evolution, d. $\delta^{66}$Zn evolution in zinc and sphalerite

In this example, as with many applications of isotope-enabled RT, there are no isotope-specific rate constant available that would uniquely constrain these constants. Rather, it is necessary to use the bulk rate constant and infer the associated values for the remaining isotopes. As a result, it is not possible here to determine the error (and thus the difference in isotopic ratio) introduced by the use of the bulk rate and the fractionation factor rather than isotopes specific rate constant as detailed by [43], [83]. As a point of reference, we illustrate the mass-weighted rate of Zn precipitated when using unique 'species' $Zn^{64}$ and $Zn^{66}$ with constants $k$ and $\alpha k$ relative to that using a single 'bulk' Zn species (no isotopes) with rate constant $k$. The sum of the initial mass of $Zn^{64}$ and $Zn^{66}$ is equal to the initial mass of the 'bulk' Zn simulation, and as described by [43], [83] there is a slight (not exceeding 5%) difference in absolute value. It is vital to appreciate that this slight difference arises because one isotope of Zn was associated with the 'bulk' rate constant $k$ while the other was associated with a slightly different constant $\alpha k$. The alternative is to assign unique values of rate constant to both isotopes, where neither are precisely equivalent to $k$, but in doing we both (1) lack uniquely determined values for these constants and (2) return to a dependence on the isotope ratio R (equation 52) which evolves over the progression of the reaction.

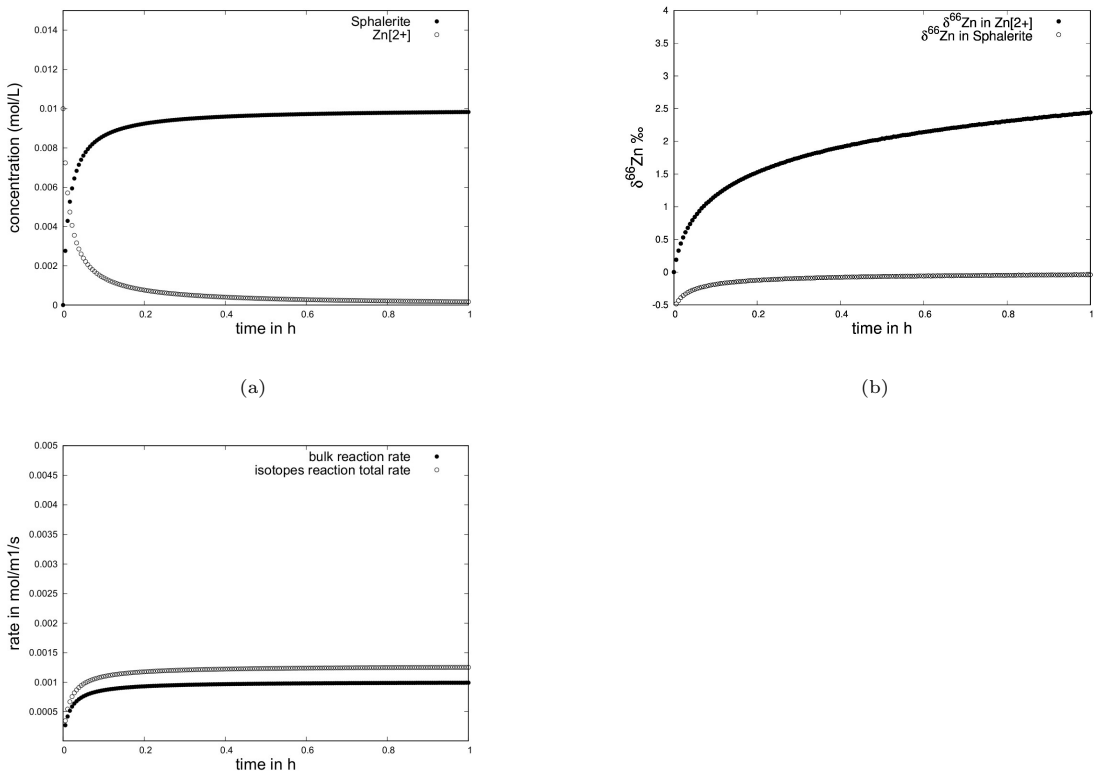


Figure 2: Simulation results during mixing: a.zinc and sphalerite evolution, b. $\delta^{66}$Zn evolution in zinc and sphalerite, c. Global rates of the bulk reaction and the isotopes dependent reaction

## 7. Conclusions

The mathematical equations defining the implementation of equilibrium and kinetic isotopic fractionation in RT codes are detailed in this paper. The classical approach is based on the hypothesis of an existing major isotope for each element of interest leading to the assumption that the constant of the isotopologue containing the major isotope is equal to the "classical" constant. In this study, we considered generic cases regarding the abundance of isotopes and the potential errors introduced when no isotope can be defined as major. We provided mathematical developments based on small deviations around enrichment factors, which are legitimate in virtually all natural systems. The calculations lead to thermodynamic constants for isotopologues depending on known thermodynamic constants and fractionation factors. Interestingly, the constants are the same as when considering major isotopes although the results stem from small deviations of $\epsilon R$ instead of negligible concentration(s) of the minor isotope(s).

This study demonstrates that no hypothesis regarding the isotopes abundances is needed to assume that the thermodynamics of one isotopologue can be defined as equal to the general thermodynamics of

the studied reaction, extending the scope of validity for this common assumption. The difference between the thermodynamic constants assigned to each isotopologue is the key for accurate modeling of isotopic fractionation.

However, we show that the same methodology has to be taken with caution when applied to kinetically driven reactions such as mineral precipitation and dissolution. As the rate constant depends on the isotopic ratio, which evolves with the progression of the reaction, an error is introduced when using the bulk rate constant and fractionation factor only when determining the isotopologue rate constants. This issue has already been highlighted in other studies investigating the question of modeling isotopic fractionation during organic compound degradation but has not been detailed in the case of minerals precipitation and dissolution reactions, which are of primary importance in a large number of reactive transport applications. The introduced error can be neglected when one isotopes of the element of interest can be considered as major, leading to small isotopic ratios. However, when modeling isotopic fractionation of elements presenting isotopes of comparable relative abundance, modelers should be aware of the introduced error depending on the methodology employed.

## 8. Acknowledgements

The authors sincerely thank the reviewer for the very relevant remark made about the mathematical developments. This comment allowed a significant improvement of the work presented in this study.

## 9. Funding

This research did not receive any specific grant from funding agencies in the public, commercial, or not-for-profit sectors.

## References

[1] Abadie, C., Lacan, F., Radic, A., Pradoux, C., and Poitrasson, F. (2017). Iron isotopes reveal distinct dissolved iron sources and pathways in the intermediate versus deep southern ocean. *Proceedings of the National Academy of Sciences*, 114(5):858–863.

[2] Acero, P., Cama, J., and Ayora, C. (2007). Sphalerite dissolution kinetics in acidic environment. *Applied Geochemistry*, 22(9):1872–1883.

[3] Almogi-Labin, A., Luz, B., and Duplessy, J.-C. (1986). Quaternary paleo-oceanography, pteropod preservation and stable-isotope record of the red sea. *Palaeogeography, Palaeoclimatology, Palaeoecology*, 57(2-4):195–211.

[4] Anderson, G. and Macqueen, R. (1982). Ore deposit models-6. mississippi valley-type lead-zinc deposits. *Geoscience Canada*.
[5] Avasarala, S., Lichtner, P. C., Ali, A.-M. S., Gonzalez-Pinzon, R., Blake, J. M., and Cerrato, J. M. (2017). Reactive transport of u and v from abandoned uranium mine wastes. *Environmental science & technology*, 51(21):12385–12393.
[6] Banner, J. L., Hanson, G., and Meyers, W. (1988). Water-rock interaction history of regionally extensive dolomites of the burlington-keokuk formation (mississippian): isotopic evidence.
[7] Banner, J. L. and Hanson, G. N. (1990). Calculation of simultaneous isotopic and trace element variations during water-rock interaction with applications to carbonate diagenesis. *Geochimica et Cosmochimica Acta*, 54(11):3123–3137.
[8] Barling, J. and Anbar, A. (2004). Molybdenum isotope fractionation during adsorption by manganese oxides. *Earth and Planetary Science Letters*, 217(3-4):315–329.
[9] Bottinga, Y. (1969). Calculated fractionation factors for carbon and hydrogen isotope exchange in the system calcite-carbon dioxide-graphite-methane-hydrogen-water vapor. *Geochimica et Cosmochimica Acta*, 33(1):49–64.
[10] Bouchez, J., Von Blanckenburg, F., and Schuessler, J. A. (2013). Modeling novel stable isotope ratios in the weathering zone. *American Journal of Science*, 313(4):267–308.
[11] Brand, U., Logan, A., Hiller, N., and Richardson, J. (2003). Geochemistry of modern brachiopods: applications and implications for oceanography and paleoceanography. *Chemical Geology*, 198(3-4):305–334.
[12] Cenki-Tok, B., Chabaux, F., Lemarchand, D., Schmitt, A.-D., Pierret, M.-C., Viville, D., Bagard, M.-L., and Stille, P. (2009). The impact of water–rock interaction and vegetation on calcium isotope fractionation in soil-and stream waters of a small, forested catchment (the strengbach case). *Geochimica et Cosmochimica Acta*, 73(8):2215–2228.
[13] Chang, V. T. C., Williams, R. J. P., Makishima, A., Belshawl, N. S., and ONions, R. K. (2004). Mg and ca isotope fractionation during caco3 biomineralisation. *Biochemical and Biophysical Research Communications*, 323(1):79–85.
[14] Cloquet, C., Carignan, J., Lehmann, M. F., and Vanhaecke, F. (2008). Variation in the isotopic composition of zinc in the natural environment and the use of zinc isotopes in biogeosciences: a review. *Analytical and bioanalytical chemistry*, 390(2):451–463.
[15] Cloquet, C., Carignan, J., Libourel, G., Sterckeman, T., and Perdrix, E. (2006). Tracing source pollution in soils using cadmium and lead isotopes. *Environmental science & technology*, 40(8):2525–2530.
[16] Corso, T. N. and Brenna, J. T. (1997). High-precision position-specific isotope analysis. *Proceedings of the National Academy of Sciences*, 94(4):1049–1053.
[17] Dasch, E. J. (1969). Strontium isotopes in weathering profiles, deep-sea sediments, and sedimentary rocks. *Geochimica et Cosmochimica Acta*, 33(12):1521–1552.
[18] De Windt, L. and Badreddine, R. (2007). Modelling of long-term dynamic leaching tests applied to solidified/stabilised waste. *Waste management*, 27(11):1638–1647.
[19] Denk, T. R., Mohn, J., Decock, C., Lewicka-Szczebak, D., Harris, E., Butterbach-Bahl, K., Kiese, R., and Wolf, B. (2017). The nitrogen cycle: A review of isotope effects and isotope modeling approaches. *Soil Biology and Biochemistry*, 105:121–137.
[20] DePaolo, D. J. (2011). Surface kinetic model for isotopic and trace element fractionation during precipitation of calcite from aqueous solutions. *Geochimica et cosmochimica acta*, 75(4):1039–1056.
[21] Druhan, J. L., Bill, M., Lim, H., Wu, C., Conrad, M. E., Williams, K. H., DePaolo, D. J., and Brodie, E. L. (2014a). A large column analog experiment of stable isotope variations during reactive transport: Ii. carbon mass balance, microbial community structure and predation. *Geochimica et Cosmochimica Acta*, 124:394–409.
[22] Druhan, J. L., Guillon, S., Lincker, M., and Arora, B. (2020). Stable and radioactive carbon isotope partitioning in soils and saturated systems: a reactive transport modeling benchmark study. *Computational Geosciences*, pages 1–11.
[23] Druhan, J. L. and Maher, K. (2014). A model linking stable isotope fractionation to water flux and transit times in heterogeneous porous media. *Procedia Earth and Planetary Science*, 10:179–188.
[24] Druhan, J. L. and Maher, K. (2017). The influence of mixing on stable isotope ratios in porous media: A revised rayleigh model. *Water Resources Research*, 53(2):1101–1124.
[25] Druhan, J. L., Steefel, C. I., Conrad, M. E., and DePaolo, D. J. (2014b). A large column analog experiment of stable isotope variations during reactive transport: I. a comprehensive model of sulfur cycling and $\delta$34s fractionation. *Geochimica et Cosmochimica Acta*, 124:366–393.
[26] Druhan, J. L., Steefel, C. I., Williams, K. H., and DePaolo, D. J. (2013). Calcium isotope fractionation in groundwater: Molecular scale processes influencing field scale behavior. *Geochimica et Cosmochimica Acta*, 119:93–116.
[27] Druhan, J. L., Winnick, M. J., and Thullner, M. (2019). Stable isotope fractionation by transport and transformation. *Reviews in Mineralogy and Geochemistry*, 85(1):239–264.
[28] Ducher, M., Blanchard, M., and Balan, E. (2016). Equilibrium zinc isotope fractionation in zn-bearing minerals from first-principles calculations. *Chemical Geology*, 443:87–96.
[29] Farmer, J. G., Eades, L. J., Mackenzie, A. B., Kirika, A., and Bailey-Watts, T. E. (1996). Stable lead isotope record of lead pollution in loch lomond sediments since 1630 ad. *Environmental Science & Technology*, 30(10):3080–3083.
[30] Fisher, J. and Boles, J. (1990). Water-rock interaction in tertiary sandstones, san joaquin basin, california, usa: diagenetic controls on water composition. *Chemical Geology*, 82:83–101.
[31] Frei, R., Paulukat, C., Bruggmann, S., and Klaebe, R. M. (2018). A systematic look at chromium isotopes in modern shells–implications for paleo-environmental reconstructions. *Biogeosciences*, 15(16):4905–4922.
[32] Gázquez, F., Columbu, A., De Waele, J., Breitenbach, S. F., Huang, C.-R., Shen, C.-C., Lu, Y., Calaforra, J.-M., Mleneck-Vautravers, M. J., and Hodell, D. A. (2018). Quantification of paleo-aquifer changes using clumped isotopes in subaqueous carbonate speleothems. *Chemical Geology*, 493:246–257.
[33] Georg, R., Reynolds, B. C., West, A., Burton, K., and Halliday, A. N. (2007). Silicon isotope variations accompanying

basalt weathering in iceland. *Earth and Planetary Science Letters*, 261(3-4):476–490.
[34] Gibson, B. D., Amos, R. T., and Blowes, D. W. (2011). 34s/32s fractionation during sulfate reduction in groundwater treatment systems: Reactive transport modeling. *Environmental science & technology*, 45(7):2863–2870.
[35] Goldstein, S. L. and Hemming, S. R. (2003). Long-lived isotopic tracers in oceanography, paleoceanography, and ice-sheet dynamics. *Treatise on geochemistry*, 6:625.
[36] Group, S. W. et al. (2007). Geotraces–an international study of the global marine biogeochemical cycles of trace elements and their isotopes. *Geochemistry*, 67(2):85–131.
[37] Hatton, J., Hendry, K., Hawkings, J., Wadham, J., Kohler, T., Stibal, M., Beaton, A., Bagshaw, E., and Telling, J. (2019). Investigation of subglacial weathering under the greenland ice sheet using silicon isotopes. *Geochimica et Cosmochimica Acta*, 247:191–206.
[38] Hendry, M., Wassenaar, L., and Kotzer, T. (2000). Chloride and chlorine isotopes (36cl and $\delta$37cl) as tracers of solute migration in a thick, clay-rich aquitard system. *Water Resources Research*, 36(1):285–296.
[39] Hindshaw, R. S., Tosca, R., Tosca, N. J., and Tipper, E. T. (2020). Experimental constraints on mg isotope fractionation during clay formation: Implications for the global biogeochemical cycle of mg. *Earth and Planetary Science Letters*, 531:115980.
[40] Hoffman, D. W. and Rasmussen, C. (2019). Position-specific carbon stable isotope ratios by proton nmr spectroscopy. *Analytical chemistry*, 91(24):15661–15669.
[41] Hunkeler, D., Abe, Y., Broholm, M. M., Jeannottat, S., Westergaard, C., Jacobsen, C. S., Aravena, R., and Bjerg, P. L. (2011). Assessing chlorinated ethene degradation in a large scale contaminant plume by dual carbon–chlorine isotope analysis and quantitative pcr. *Journal of contaminant hydrology*, 119(1-4):69–79.
[42] Hunkeler, D., Aravena, R., Parker, B., Cherry, J., and Diao, X. (2003). Monitoring oxidation of chlorinated ethenes by permanganate in groundwater using stable isotopes: Laboratory and field studies. *Environmental Science & Technology*, 37(4):798–804.
[43] Hunkeler, D., Van Breukelen, B. M., and Elsner, M. (2009). Modeling chlorine isotope trends during sequential transformation of chlorinated ethenes. *Environmental science & technology*, 43(17):6750–6756.
[44] Lagneau, V., Regnault, O., and Descostes, M. (2019). Industrial deployment of reactive transport simulation: an application to uranium in situ recovery. *Review in Mineralogy and Geochemistry*.
[45] Larson, P. B., Maher, K., Ramos, F. C., Chang, Z., Gaspar, M., and Meinert, L. D. (2003). Copper isotope ratios in magmatic and hydrothermal ore-forming environments. *Chemical Geology*, 201(3-4):337–350.
[46] Lasaga, A. C. (1984). Chemical kinetics of water-rock interactions. *Journal of geophysical research: solid earth*, 89(B6):4009–4025.
[47] Lawrence, J. and Taylor Jr, H. (1972). Hydrogen and oxygen isotope systematics in weathering profiles. *Geochimica et Cosmochimica Acta*, 36(12):1377–1393.
[48] Leach, D., MACQUAR, J.-C., Lagneau, V., Leventhal, J., Emsbo, P., and Premo, W. (2006). Precipitation of lead–zinc ores in the mississippi valley-type deposit at trèves, cévennes region of southern france. *Geofluids*, 6(1):24–44.
[49] Leach, D. L., Bradley, D., Lewchuk, M. T., Symons, D. T., de Marsily, G., and Brannon, J. (2001). Mississippi valley-type lead–zinc deposits through geological time: implications from recent age-dating research. *Mineralium Deposita*, 36(8):711–740.
[50] Lemarchand, D., Gaillardet, J., Lewin, E., and Allegre, C. (2002). Boron isotope systematics in large rivers: implications for the marine boron budget and paleo-ph reconstruction over the cenozoic. *Chemical Geology*, 190(1-4):123–140.
[51] Li, L., Steefel, C. I., Williams, K. H., Wilkins, M. J., and Hubbard, S. S. (2009). Mineral transformation and biomass accumulation associated with uranium bioremediation at rifle, colorado. *Environmental science & technology*, 43(14):5429–5435.
[52] Lichtner, P. and Seth, M. (1996). Multiphase multicomponent nonisothermal reactive transport in partially saturated porous media. In *Proceedings of the 1996 international conference on deep geological disposal of radioactive waste*.
[53] Lichtner, P. C. (1996). Continuum formulation of multicomponent-multiphase reactive transport. *Reviews in mineralogy*, 34:1–82.
[54] Maher, K. and Navarre-Sitchler, A. (2019). Reactive transport processes that drive chemical weathering: From making space for water to dismantling continents. *Reviews in Mineralogy and Geochemistry*, 85(1):349–380.
[55] Maher, K., Steefel, C. I., DePaolo, D. J., and Viani, B. E. (2006). The mineral dissolution rate conundrum: Insights from reactive transport modeling of u isotopes and pore fluid chemistry in marine sediments. *Geochimica et Cosmochimica Acta*, 70(2):337–363.
[56] Maréchal, C. N., Télouk, P., and Albarède, F. (1999). Precise analysis of copper and zinc isotopic compositions by plasma-source mass spectrometry. *Chemical geology*, 156(1-4):251–273.
[57] Mathur, R., Titley, S., Barra, F., Brantley, S., Wilson, M., Phillips, A., Munizaga, F., Maksaev, V., Vervoort, J., and Hart, G. (2009). Exploration potential of cu isotope fractionation in porphyry copper deposits. *Journal of Geochemical exploration*, 102(1):1–6.
[58] Migeon, V., Bourdon, B., Pili, E., and Fitoussi, C. (2018). Molybdenum isotope fractionation during acid leaching of a granitic uranium ore. *Geochimica et Cosmochimica Acta*, 231:30–49.
[59] Mook, W. G., Bommerso.Jc, and Staverma.Wh (1974). Carbon isotope fractionation between dissolved bicarbonate and gaseous carbon-dioxide. *Earth and Planetary Science Letters*, 22(2):169–176.
[60] Nestler, A., Berglund, M., Accoe, F., Duta, S., Xue, D., Boeckx, P., and Taylor, P. (2011). Isotopes for improved management of nitrate pollution in aqueous resources: review of surface water field studies. *Environmental Science and Pollution Research*, 18(4):519–533.
[61] Oelkers, E. H., Butcher, R., Pogge von Strandmann, P. A. E., Schuessler, J. A., von Blanckenburg, F., Snaebjörnsdóttir,

S. O., Mesfin, K., Aradóttir, E. S., Gunnarsson, I., Sigfússon, B., Gunnlaugsson, E., Matter, J. M., Stute, M., and Gislason, S. R. (2019). Using stable mg isotope signatures to assess the fate of magnesium during the in situ mineralisation of co2 and h2s at the carbfix site in sw-iceland. *Geochimica et Cosmochimica Acta*, 245:542–555.

[62] Pichat, S., Douchet, C., and Albarède, F. (2003). Zinc isotope variations in deep-sea carbonates from the eastern equatorial pacific over the last 175 ka. *Earth and Planetary Science Letters*, 210(1-2):167–178.

[63] Pistiner, J. S. and Henderson, G. M. (2003). Lithium-isotope fractionation during continental weathering processes. *Earth and Planetary Science Letters*, 214(1-2):327–339.

[64] Remaud, G. S., Julien, M., Parinet, J., Nun, P., Robins, R. J., and Höhener, P. (2015). Position-specific isotope analysis by isotopic nmr spectrometry: New insights on environmental pollution studies. *Procedia Earth and Planetary Science*, 13:92–95.

[65] Rogers, K. M. (2003). Stable carbon and nitrogen isotope signatures indicate recovery of marine biota from sewage pollution at moa point, new zealand. *Marine pollution bulletin*, 46(7):821–827.

[66] Rozanski, K., Johnsen, S. J., Schotterer, U., and Thompson, L. (1997). Reconstruction of past climates from stable isotope records of palaeo-precipitation preserved in continental archives. *Hydrological sciences journal*, 42(5):725–745.

[67] Schmitt, A.-D., Gangloff, S., Labolle, F., Chabaux, F., and Stille, P. (2017). Calcium biogeochemical cycle at the beech tree-soil solution interface from the strengbach czo (ne france): insights from stable ca and radiogenic sr isotopes. *Geochimica et Cosmochimica Acta*, 213:91–109.

[68] Sherman, L. S., Blum, J. D., Dvonch, J. T., Gratz, L. E., and Landis, M. S. (2015). The use of pb, sr, and hg isotopes in great lakes precipitation as a tool for pollution source attribution. *Science of the Total Environment*, 502:362–374.

[69] Shouakar-Stash, O., Alexeev, S., Frape, S., Alexeeva, L., and Drimmie, R. (2007). Geochemistry and stable isotopic signatures, including chlorine and bromine isotopes, of the deep groundwaters of the siberian platform, russia. *Applied geochemistry*, 22(3):589–605.

[70] Sigman, D. M., Karsh, K., and Casciotti, K. (2009). Ocean process tracers: nitrogen isotopes in the ocean.

[71] Sin, I., Lagneau, V., De Windt, L., and Corvisier, J. (2017). 2d simulation of natural gas reservoir by two-phase multicomponent reactive flow and transport - description of a benchmarking exercise. *Mathematics and Computers in Simulation*, 137:431–447.

[72] Singleton, M. J., Sonnenthal, E. L., Conrad, M. E., DePaolo, D. J., and Gee, G. W. (2004). Multiphase reactive transport modeling of seasonal infiltration events and stable isotope fractionation in unsaturated zone pore water and vapor at the hanford site. *Vadose Zone Journal*, 3(3):775–785.

[73] Sprenger, M., Leistert, H., Gimbel, K., and Weiler, M. (2016). Illuminating hydrological processes at the soil-vegetation-atmosphere interface with water stable isotopes. *Reviews of Geophysics*, 54(3):674–704.

[74] Steefel, C., Appelo, C., Arora, B., Jacques, D., Kalbacher, T., Kolditz, O., Lagneau, V., Lichtner, P., Mayer, K. U., Meeussen, J., et al. (2015). Reactive transport codes for subsurface environmental simulation. *Computational Geosciences*, 19(3):445–478.

[75] Steefel, C. and Lichtner, P. (1998a). Multicomponent reactive transport in discrete fractures: Ii: Infiltration of hyperalkaline groundwater at maqarin, jordan, a natural analogue site. *Journal of Hydrology*, 209(1-4):200–224.

[76] Steefel, C. I., Druhan, J. L., and Maher, K. (2014). Modeling coupled chemical and isotopic equilibration rates. *Procedia Earth and Planetary Science*, 10:208–217.

[77] Steefel, C. I. and Lichtner, P. C. (1998b). Multicomponent reactive transport in discrete fractures: I. controls on reaction front geometry. *Journal of Hydrology*, 209(1-4):186–199.

[78] Thomas, D. J., Bralower, T. J., and Jones, C. E. (2003). Neodymium isotopic reconstruction of late paleocene–early eocene thermohaline circulation. *Earth and Planetary Science Letters*, 209(3-4):309–322.

[79] Thorstenson, D. C. and Parkhurst, D. L. (2004). Calculation of individual isotope equilibrium constants for geochemical reactions. *Geochimica et cosmochimica acta*, 68(11):2449–2465.

[80] Urey, H. C. (1947). The thermodynamic properties of isotopic substances. *Journal of the Chemical Society (Resumed)*, pages 562–581.

[81] van Breukelen, B. M., Griffioen, J., Röling, W. F., and van Verseveld, H. W. (2004). Reactive transport modelling of biogeochemical processes and carbon isotope geochemistry inside a landfill leachate plume. *Journal of Contaminant Hydrology*, 70(3-4):249–269.

[82] Van Breukelen, B. M., Hunkeler, D., and Volkering, F. (2005). Quantification of sequential chlorinated ethene degradation by use of a reactive transport model incorporating isotope fractionation. *Environmental science & technology*, 39(11):4189–4197.

[83] Van Breukelen, B. M., Thouement, H. A., Stack, P. E., Vanderford, M., Philp, P., and Kuder, T. (2017). Modeling 3d-csia data: Carbon, chlorine, and hydrogen isotope fractionation during reductive dechlorination of tce to ethene. *Journal of contaminant hydrology*, 204:79–89.

[84] Van der Lee, J. (1998). Thermodynamic and mathematical concepts of chess.

[85] Van Der Lee, J., De Windt, L., Lagneau, V., and Goblet, P. (2003). Module-oriented modeling of reactive transport with hytec. *Computers & Geosciences*, 29(3):265–275.

[86] Veeramani, H., Eagling, J., Jamieson-Hanes, J. H., Kong, L., Ptacek, C. J., and Blowes, D. W. (2015). Zinc isotope fractionation as an indicator of geochemical attenuation processes. *Environmental Science & Technology Letters*, 2(11):314–319.

[87] Wanner, C., Druhan, J. L., Amos, R. T., Alt-Epping, P., and Steefel, C. I. (2015). Benchmarking the simulation of cr isotope fractionation. *Computational geosciences*, 19(3):497–521.

[88] Wanner, C., Eggenberger, U., and Mäder, U. (2012). A chromate-contaminated site in southern switzerland–part 2: Reactive transport modeling to optimize remediation options. *Applied geochemistry*, 27(3):655–662.

[89] Wanner, C. and Sonnenthal, E. L. (2013). Assessing the control on the effective kinetic cr isotope fractionation factor: A reactive transport modeling approach. *Chemical geology*, 337:88–98.

[90] Wanner, P., Parker, B. L., Chapman, S. W., Aravena, R., and Hunkeler, D. (2016). Quantification of degradation of chlorinated hydrocarbons in saturated low permeability sediments using compound-specific isotope analysis. *Environmental science & technology*, 50(11):5622–5630.